TU Delft

Delft University of Technology

Document Version
Final published version

Licence
CC BY-NC-ND

Citation (APA)
Lont, Y., Steinmann, P., Kwakkel, J., & Comes, T. (2026). How advanced information technologies help and hurt adaptation in crisis-response supply chains. *International Journal of Disaster Risk Reduction*, *145*, Article 106342. https://doi.org/10.1016/j.ijdrr.2026.106342

Important note
To cite this publication, please use the final published version (if applicable).
Please check the document version above.

Copyright
In case the licence states “Dutch Copyright Act (Article 25fa)”, this publication was made available Green Open Access via the TU Delft Institutional Repository pursuant to Dutch Copyright Act (Article 25fa, the Taverne amendment). This provision does not affect copyright ownership.
Unless copyright is transferred by contract or statute, it remains with the copyright holder.

Sharing and reuse
Other than for strictly personal use, it is not permitted to download, forward or distribute the text or part of it, without the consent of the author(s) and/or copyright holder(s), unless the work is under an open content license such as Creative Commons.

Takedown policy
Please contact us and provide details if you believe this document breaches copyrights.
We will remove access to the work immediately and investigate your claim.

This work is downloaded from Delft University of Technology.

Journal of Physics:
Conference Series

PURPOSE-LED PUBLISHING™

PAPER • OPEN ACCESS

Data-Driven Wave Feedforward Control for Floating Offshore Wind Turbines

To cite this article: Leendert Starink *et al* 2026 *J. Phys.: Conf. Ser.* **3224** 082001

View the article online for updates and enhancements.

You may also like

- Feedforward control for wave disturbance rejection on floating offshore wind turbines
M. Al, A. Fontanella, D. van der Hoek et al.
- Design Optimization of Spar Floating Wind Turbines Considering Different Control Strategies
John Marius Hegseth, Erin E. Bachynski and Joaquim R. R. A. Martins
- Balancing rotor speed regulation and drive train loads of floating wind turbines
Boris Fischer and Peter Loepelmann

Enabling Electrochemistry Inside and Outside the Lab

PalmSens

Discover our diverse range of Potentiostats engineered to support your research wherever it takes you

- Intuitive software for Windows and Android
- Proven in over 4000 scientific publications
- Single-channel and multi-channel
- Benchtop, portable and wearable

Discover More



This content was downloaded from IP address 131.180.130.140 on 03/11/2026 at 10:52

Journal of Physics: Conference Series **3224** (2026) 082001 doi:10.1088/1742-6596/3224/8/082001

Data-Driven Wave Feedforward Control for Floating Offshore Wind Turbines

Leendert Starink[1], **Sebastiaan Mulders**[1] **and Jan-Willem van Wingerden**[1]

[1]DCSC, Delft University of Technology, Delft, the Netherlands

E-mail: `l.starink@tudelft.nl`

Abstract. The development of floating wind energy is necessary to expand offshore wind energy to deeper waters. From a control perspective, floating wind turbines pose interesting new challenges. Among these challenges is the mitigation of wave disturbances, which occur above the bandwidth of the collective pitch feedback controller. Therefore, wave feedforward control has been proposed, which uses a radar to estimate a preview of the wave loads acting on the platform. To obtain optimally calibrated wave feedforward controllers of user-defined complexity, this work proposes a data-driven approach that integrates model-based insights with the iterative feedback tuning (IFT) algorithm. The approach balances rotor speed tracking and platform pitching motion in its performance criterion. To assess the performance of the proposed approach, the frequency response of the optimal wave feedforward controller is derived and identified, and the IFT calibrated controllers are compared to this controller. It is shown that the method is effective in calibrating the controller to a trade off between mitigating platform pitching motion, and rotor speed tracking, and it is demonstrated that the data-driven controller approaches the performance of the optimal controller.

1. Introduction

Wind energy has become the leading source of renewable energy in Europe. Over the next decades, the total installed capacity for wind energy is planned to grow from the current 35 GW, to 60 GW in 2030, and 300 GW in 2050 [1]. To facilitate this growth, there is a need for suitable installation sites for future wind farms. The majority of offshore sites in Europe with favorable conditions to wind energy are located in areas with water depths exceeding 60 meters [2], where the installation of bottom-fixed wind turbines is uneconomical. Therefore, to access these resources, floating wind turbines (FWTs) are crucial.

The control of FWTs poses new challenges. Compared to bottom-fixed turbines, FWTs have the additional degrees of freedom of the floater. Concretely, the interaction of the platform pitching motion with the collective pitch controller designed for bottom-fixed turbines results in instability, and is referred to as the negative damping problem [3]. In addition, FWTs are subject to wave disturbances, which are concentrated at higher frequencies than wind disturbances, and are typically outside the bandwidth of the feedback controller.

As a result, there is a need to develop FWT controllers capable of mitigating higher-frequency disturbances. To this end, wave feedforward control has been proposed, where the approach is to use radar measurements of the incoming wave-field to estimate the wave loads that act on the platform [4]. Currently, one data-driven approach that uses data-enabled predictive

Content from this work may be used under the terms of the Creative Commons Attribution 4.0 licence. Any further distribution of this work must maintain attribution to the author(s) and the title of the work, journal citation and DOI.
Published under licence by IOP Publishing Ltd

control exists [5], and several model-based approaches have been proposed, e.g. [6, 7] and [8]. Both model-based, and data-driven approaches have drawbacks. The data-driven approach requires solving a computationally expensive online optimization problem, and on the other side, obtaining a good model for the model-based design of a wave feedforward controller is challenging, as the dynamics of FWTs are the result of complex interactions of many degrees of freedom.

The motivation of this work is to integrate model-based and data-driven techniques, by using identification experiments on a simulator to design the structure of a parametric controller, and use iterative feedback tuning (IFT) [9] to calibrate the parameters of this controller with experiments on the real system. The benefit of this approach, is that model-based insights allow to select a controller structure of limited complexity, and the IFT algorithm mitigates the effect of modeling errors on the performance of the controller in a data-driven manner.

The contribution of this work is threefold. The first contribution is an approach for obtaining wave feedforward controllers that integrates model-based and data-driven techniques, and that yields an optimally calibrated controller of user-defined complexity. The second contribution is that this approach is used to explore wave feedforward controller designs that trade off rotor speed tracking performance, and the mitigation of platform pitching motion. The third contribution is the derivation of an optimal wave feedforward controller with use of frequency domain identification techniques, with which the accuracy of the proposed method is demonstrated.

The remainder of this work is structured as follows. Section 2 provides the methodology of this work, where first an optimal control problem is formulated, second, the controller structure and parameterization is designed using identification experiments, and third, the IFT algorithm is introduced. The results are presented in Section 3, and the paper is concluded in Section 4.

2. Methodology

The proposed approach to obtain an optimally calibrated controller of user defined structure consists of two steps: 1) performing identification experiments on a high-fidelity simulator to determine an appropriate controller structure, and 2) use IFT on the physical system to calibrate the controller parameters. The motivation is that the optimal controller structure is assumed to be consistent between a high-fidelity simulator and the physical system, as the governing dynamics are modeled in the simulator. However, the optimal controller parameters can vary between the simulator and the physical system, e.g. due to discrepancies in the true natural frequencies and the natural frequencies of the model.

The objective of this work is to demonstrate that once a controller structure has been determined, the IFT algorithm converges to the optimal controller calibration within a reasonable number of iterations, and with experiments conducted under realistic environmental conditions. To show this, both the identification, and the IFT step are performed on the IEA 15MW turbine on the VolturnUS-S platform, simulated in the QBlade simulation environment [10]. As an effect, there is no modeling discrepancy between the identification experiments and the data-driven calibration, and hence the optimal controller parameters are already obtained in the identification step. The knowledge of the optimal controller parameters allows to perform a convergence study for the IFT algorithm. This is achieved by initializing the algorithm with parameters that are randomly perturbed from their optimal value. With this convergence study, the performance and accuracy of the algorithm is evaluated, and it is shown that the IFT calibrated controller converges to close proximity of the optimally calibrated controller, within reasonable time, and while subject to disturbances originating from turbulence and waves.

The methodology of this work is graphically summarized in Fig. 1. It is illustrated that the controller structure is determined using identification experiments and empirical transfer

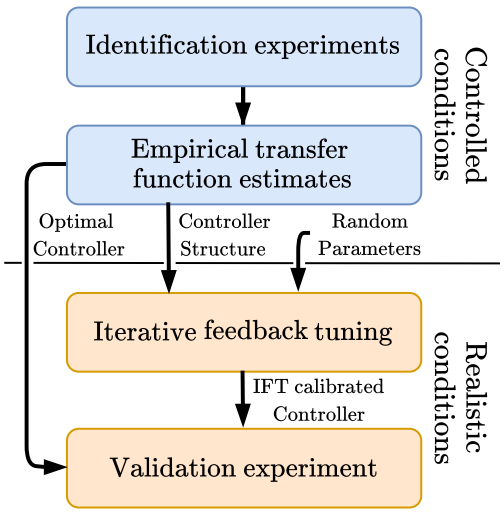


Figure 1: Overview of the methodology of this work, illustrating that identification experiments in controlled conditions are used to obtain a controller structure and parameterization, and to estimate the optimal wave feedforward controller. Next, the IFT algorithm is initialized with random parameters, and calibrates these parameters in realistic conditions. The optimal controller, and the IFT calibrated controller are compared in a validation experiment.

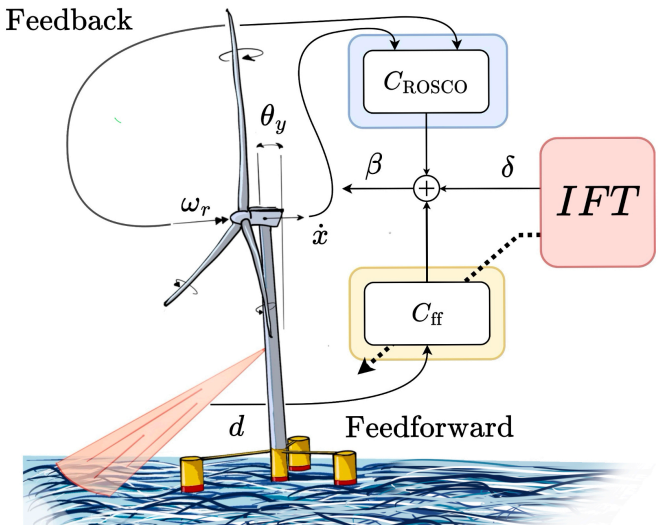


Figure 2: Schematization of the control architecture, illustrating a floating wind turbine equipped with a radar. The radar scans the incoming wave field to estimate the moment d the waves exert on the platform. From the turbine, the rotor speed ω_{r}, the platform pitch angle θ_y, and the tower top velocity $\dot{x}$ are measured. The turbine is controlled with the collective pitch angle β, which is obtained from the feedback controller C_{ROSCO}, and the wave feedforward controller C_{ff}. The wave feedforward controller is calibrated by the IFT algorithm, which uses the signal δ to perform excitation experiments.

function estimates (ETFEs), after which IFT algorithm receives the controller structure, and calibrates the controller parameters. To obtain the optimal controller, the identification experiments are conducted under controlled conditions. Several experiments are conducted in which the dynamics induced by pitch actuation, wind disturbances and wave disturbances are analyzed separately, and with no limitation on the experiment duration, thereby creating an ideal environment for system identification. To test the performance of the IFT algorithm, the IFT experiments are conducted under realistic conditions, by considering turbulent inflow, waves, and with limited experiment duration. The IFT algorithm is initialized with random parameters, and the result of multiple runs is compared to assess the convergence of the algorithm.

The remainder of this section is structured as follows. Wave feedforward control is defined as an optimal control problem in Section 2.1, Section 2.2 covers the identification procedure, and designs an adequate controller structure, after which Section 2.3 introduces the IFT algorithm.

2.1. Problem definition for wave feedforward control

This section provides a general analysis of wave feedforward control, and has the goal to condense this into an optimal control problem. To obtain an optimal control problem, first the control architecture, and the relevant signals need to be considered, which are shown in Fig. 2. In the figure, an FWT is illustrated that is outfitted with a radar that scans the incoming wave field. From the turbine, the rotor speed ω_{r}, the platform pitching motion θ_y, and the fore-aft nacelle velocity $\dot{x}$ are measured, and the collective pitch angle β is available for control. The collective

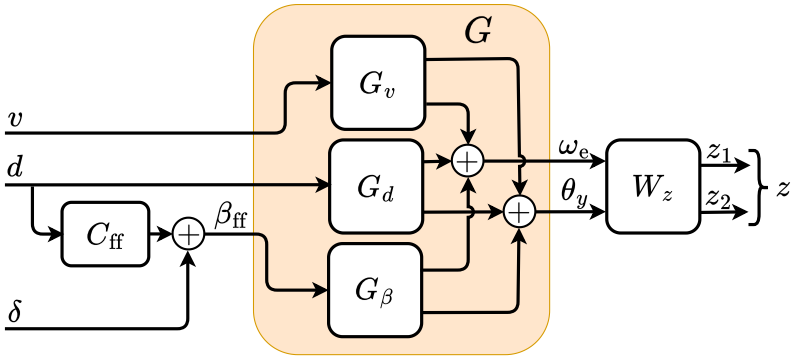


Figure 3: Block diagram of the system. The interconnection of the FWT and the ROSCO feedback controller is abstracted to the transfer function matrix $G \in \mathbb{C}^{3\times 2}$. In turn, G is partitioned as $\{G_v, G_d, G_\beta\} \in \mathbb{C}^{2\times 1}$, which describe the dynamics from the wind disturbance, the wave disturbance, and the feedforward pitch angle, to the rotor speed error and the platform pitch motion, respectively. At the output of the system, the transfer function matrix $W_z(s) \in \mathbb{C}^{2\times 2}$ provides frequency weighing, and outputs the performance channels z.

pitch angle is obtained by adding the output of the feedforward controller C_{ff}, and the ROSCO controller [11], which is used as feedback controller. The ROSCO controller uses the rotor speed and the tower top velocity for feedback. The feedforward controller acts on an estimate of the pitching moment exerted on the platform by the waves d. Recent work has shown that this quantity can be accurately estimated from radar information [4, 12]. For the simulations performed in this work, the pitching moment is assumed to be known, and the direction of the waves is aligned with the wind direction.The feedforward controller takes the form of a transfer function, and is parameterized by the parameter vector $\rho \in \mathbb{R}^n$. This parameter vector is subject to tuning by the IFT algorithm, which manipulates the signal δ to perform excitation experiments.

For analysis purposes, Figure 3 abstracts the system into a block diagram. In this block diagram, the turbine is represented by the linear time invariant (LTI) transfer function matrix $G(s) \in \mathbb{C}^{2\times 3}$, which is partitioned into the three systems $\{G_v, G_d, G_\beta\} \in \mathbb{C}^{2\times 1}$. These systems describe the dynamics from the wind disturbance v, the wave disturbance d, and the feedforward collective pitch signal β_{ff}, to the outputs of interest; the platform pitch angle θ_y and the rotor speed tracking error ω_{e}, respectively. Note that the ROSCO feedback controller is included in these dynamics, and that these systems hence describe the closed-loop dynamics of the turbine. At the output, the user defined filter $W_z(s) \in \mathbb{C}^{2\times 2}$ provides frequency weighing to the outputs, to result in the performance channels $z \in \mathbb{R}^2$. Because wave disturbances generally occur at higher frequencies than wind disturbances, the frequency weight is designed as

$$W_z(s) = \frac{s^2}{s^2 + 2\zeta_{\text{w}}\omega_{\text{w}}s + \omega_{\text{w}}^2} \cdot \begin{bmatrix} 1 & 0 \\ 0 & 1 \end{bmatrix}, \tag{1}$$

where $\zeta_{\text{w}} = 0.7$ and $\omega_{\text{w}} = 0.3$ rad/s parameterize a high-pass filter with a cut-in frequency slightly below the lowest frequency in the wave spectrum. As a result, the contribution of wind disturbances on the performance channels are mitigated. Using Fig. 3, the performance channels are expressed as

$$z(t,\rho) = W_z \begin{bmatrix} G_v & G_d & G_\beta \end{bmatrix} \begin{bmatrix} v(t) & d(t) & C_{\text{ff}}(\rho)d(t) + \delta(t) \end{bmatrix}^\top. \tag{2}$$

With the performance channels defined, it is possible to define the cost function

$$J(\rho) = \mathbf{E}\big[z(t,\rho)^\top W z(t,\rho)\big] \triangleq \lim_{T\to\infty}\left[\frac{1}{T}\int_0^T z(t,\rho)^\top W z(t,\rho)dt\right], \tag{3}$$

where $\mathbf{E}$ denotes the expected value, W is a weighting matrix, and the cost is a function of the controller parameters. It is the interest of this work to calibrate feedforward controllers to optimize a trade-off between the performance channels, therefore the weighting matrix is

$$W(\alpha) = \begin{bmatrix}\alpha & 0\\ 0 & \kappa(1-\alpha)\end{bmatrix}, \tag{4}$$

where $\alpha \in [0,1]$ determines the trade-off between the channels, and $\kappa = 0.2$, is a fixed scaling variable to ensure that the signals have the same order of magnitude. By optimizing this cost function for various α, it is possible to investigate the trade-off between rejecting the wave disturbance from the rotor speed, and from the platform pitching motion.

2.2. Identification for controller structure design
The objective of this section is to design an appropriate structure and parameterization for the feedforward controller, such that this can be provided to the IFT algorithm. To this end this section is divided in three subsections. Section 2.2.1 analyzes the cost function in the frequency domain, and obtains an analytic expression for the frequency response of the optimal feedforward controller in terms of the unknown system dynamics, and the performance weights. Section 2.2.2 identifies the required system dynamics, and uses these to compute the frequency response of the optimal controller. Section 2.2.3 analyzes the obtained frequency response to design an appropriate controller structure, and computes the optimal controller parameters given these estimates, by solving a weighted least-squares problem.

2.2.1. The optimal non-parametric controller To derive the optimal frequency response, observe that under mild assumptions the cost function has a frequency domain equivalent

$$J(\alpha, C_{\text{ff}}(j\omega)) = \lim_{T\to\infty}\frac{1}{2\pi T}\int_{-\infty}^{\infty} Z_T^*(j\omega, C_{\text{ff}}(j\omega))W(\alpha)Z_T(j\omega, C_{\text{ff}}(j\omega))d\omega, \tag{5}$$

which follows from Parseval's relation, and where $Z_T(j\omega)$ denotes the Fourier transform of $z(t)$ based on a time window T, and $(\cdot)^*$ denotes the complex conjugate transpose. Note that the cost function is expressed as a function of the frequency response $C_{\text{ff}}(j\omega)$, rather than the controller parameters, because it is the goal to obtain a non-parametric estimate of the optimal frequency response. The benefit of treating the problem in the frequency domain, is that the responses at different frequencies can be minimized independently, and the problem reduces to a quadratic optimization problem which, under the assumption that v and d are uncorrelated, has the closed-form solution

$$\bar{C}_{\text{ff}}(j\omega,\alpha) = \big[G_\beta^*(j\omega)\mathcal{W}(j\omega,\alpha)G_\beta(j\omega)\big]^{-1} G_\beta^*(j\omega)\mathcal{W}(j\omega,\alpha)G_d(j\omega), \tag{6}$$

where $\mathcal{W}(j\omega,\alpha) = W_z^*(j\omega)W(\alpha)W_z(j\omega)$ is the frequency dependent weight, and the overline denotes that this is the non-parametric optimal feedforward controller.

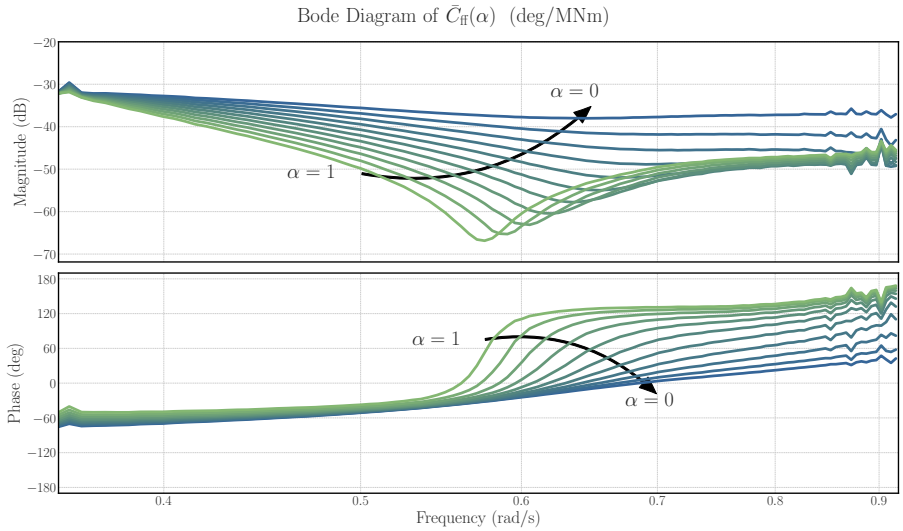


Figure 4: Bode diagram of the optimal non-parametric feedforward controllers for varying α. The difference in frequency responses is predominantly determined by a zero, which for $\alpha = 1$ has a dominant presence in frequency response. The effect of the zero becomes smaller as α tends to zero, and shifts to higher frequencies

2.2.2. Identification experiments From the derivation in the previous section it is clear that the frequency response of the optimal feedforward controller is expressed as a function of $G_\beta(j\omega)$ and $G_d(j\omega)$. Therefore, following the method used in [6], frequency domain estimates of these transfer functions are made with use of ETFEs. While [6] used this methodology to explore the limit cases, i.e. $\alpha = 0$ and 1, by using (6), this work also explores the trade-off by considering intermediate values of α.

To estimate the frequency responses $G_\beta(j\omega)$ and $G_d(j\omega)$, two experiments with a duration of $50 \cdot 10^3$ seconds are simulated. First, to estimate G_d, the FWT is simulated with a constant wind speed of 16 m/s, and with measured wave disturbances $d_{\text{exp1}}(t)$. Second, to estimate G_β, the FWT is simulated with constant wind speed, no wave disturbances, and where a chirp signal $f_{\text{exp2}}(t)$, that is logarithmically distributed over the frequency range $[0.01, 0.5]$ Hz, and with a pitch amplitude of 2.5 degrees, is supplied to the channel δ to excite the collective pitch angle. From these experiments, ETFEs are constructed as

$$\widehat{G}_d(j\omega) = \frac{Z_{\text{exp1}}(j\omega)D^*_{\text{exp1}}(j\omega)}{|D_{\text{exp1}}(j\omega)|^2}, \quad \text{and} \quad \widehat{G}_\beta(j\omega) = \frac{Z_{\text{exp2}}(j\omega)F^*_{\text{exp2}}(j\omega)}{|F^*_{\text{exp2}}(j\omega)|^2}, \tag{7}$$

where $Z_{\text{exp1}}, Z_{\text{exp2}}, D_{\text{exp2}}$ and F_{exp2} are the discrete time Fourier transforms of the performance channels during both experiments, the wave moment, and the chirp signal, respectively.

2.2.3. The parametric controller The ETFEs of (7) are used in (6) to compute the optimal non-parametric feedforward controller for different α. Using these non-parametric controllers, a controller structure is designed in this section. A Bode diagram of the obtained frequency responses is presented in Fig. 4, where only the frequency region where the wave disturbance contains power is shown. The magnitude responses indicate that for $\alpha = 1$, the response contains a zero at approximately .57 rad/s. The effect of this zero becomes less dominant for smaller α, and shifts to higher frequencies. This effect is also reflected in the phase response, which is approximately $-90°$ for low frequencies for all α, after which the phase responses diverge beyond

the frequency associated to the zero. Based on these observations the controller structure is designed as

$$C_{\text{ff}}(\rho) = k\left(\frac{s^2 + 2\omega_{\text{n}}\zeta_{\text{n}}s + \omega_{\text{n}}^2}{s^2 + 2\omega_{\text{d}}\zeta_{\text{d}}s + \omega_{\text{d}}^2}\right)\left(\frac{s+n}{s+p}\right), \quad \rho = [k \quad \omega_{\text{n}} \quad \zeta_{\text{n}}]^\top, \tag{8}$$

consisting of a gain k, a complex conjugate zero pair parameterized by a damping coefficient ζ_{n} and natural frequency ω_{n}, a low-pass filter parameterized by ζd and ω_{d}, and a lead-lag filter parameterized by n and p. From Fig. 4, the zero pair and the controller gain are identified as the most important tuning parameters, and hence these parameters are included in ρ, and are subject to tuning by the IFT algorithm. The lead-lag filter is manually tuned to facilitate the $-90°$ phase at low frequencies, and the low-pass filter is included to make the controller causal.

Finally, to provide a benchmark to the IFT calibrated controllers, the optimal controller parameters given the estimates in (7) are computed by solving a weighted least-squares problem

$$\rho_{\text{opt}}(\alpha) = \arg\min \sum_{\omega\in\Omega} S_d(j\omega) \left\|\bar{C}_{\text{ff}}(\alpha, j\omega) - C_{\text{ff}}(\rho, j\omega)\right\|_2^2, \tag{9}$$

where $S_d(j\omega)$ is the power spectrum of d, and Ω denotes the discrete frequencies that are available from the ETFEs.

2.3. Iterative feedback tuning

This section introduces the IFT algorithm, which is used to calibrate the controller parameters of the controller designed in the previous section. The IFT algorithm is an iterative algorithm, that facilitates an iterative gradient-based optimization scheme to calibrate the controller parameters. The algorithm requires two experiments per iteration, which allow to make unbiased estimates of the cost function, and the cost function gradient with respect to the controller parameters. With this information a gradient-based optimization scheme is implemented to update the controller parameters. While conventionally the algorithm is developed for a two degree-of-freedom control structure, in this work only the feedforward controller is subject to tuning. For an elaborate overview of the algorithm, the reader is referred to the work of H. Hjalmarsson in [9].

The iterative tuning procedure consists of three steps: 1) a first experiment to make an estimate of the cost function for a given set of controller parameters, 2) a second experiment to estimate the cost function gradient, and 3) an update of the controller parameters using an optimization scheme, after which the procedure is repeated. To denote to which experiment, and to what iteration a variable or signal belongs, this work adopts subscripts and superscripts, such that z_j^i originates from the j^{th} experiment of the i^{th} iteration. For clarity in notation, the superscript is omitted whenever there is no risk of confusion.

2.3.1. First experiment This experiment collects signals from the system operating under normal conditions. Hence, referring to (2), from this experiment

$$z_1(\rho^i) = W_z\left[\left(G_\beta C_{\text{ff}}(\rho^i) + G_d\right) d_1(t) + G_v v_1(t)\right], \tag{10}$$

is measured. Using these signals, a finite sample estimate of the cost function is made

$$\hat{J}_N(\rho^i) = \frac{1}{N}\sum_{k=0}^{N-1} {z_1}^\top(k, \rho^i) W z_1(k, \rho^i), \tag{11}$$

where N is the number of samples in the experiment. In this work, the experiment duration is set to 60 seconds, and the sampling frequency is 40 Hz, resulting in $N = 2400$.

2.3.2. Second experiment The second experiment estimates the gradient of the cost function by performing an excitation experiment, and is hence referred to as the gradient experiment. To this end, the algorithm uses the channel δ, see Figs. 2 and 3, to inject a signal at the process input. To show how this is used to obtain the desired gradient estimate, (11) is differentiated with respect to the controller parameters

$$\frac{\partial J_N}{\partial \rho}(\rho^i) = \frac{2}{N}\sum_{k=0}^{N} \frac{\partial z_1}{\partial \rho}^{\top}(k,\rho^i) W z_1(k,\rho^i), \tag{12}$$

showing that to obtain the cost function gradient, the signal $\partial z_1/\partial\rho$ is required. Therefore, (10) is differentiated with respect to the controller parameters to obtain

$$\frac{\partial z_1}{\partial \rho}(\rho^i) = \frac{\partial C_{\text{ff}}}{\partial \rho}(\rho^i) W_z G_\beta d_1. \tag{13}$$

By carefully looking at this equation, this shows that if the wave disturbance d_1, that was measured during the first experiment, is supplied at the input of the system, the desired gradient signal is obtained by filtering the output with $\partial C/\partial\rho$. Therefore, for the second experiment $\delta_2 = Kd_1$, which results in

$$z_2(\rho^i) = W_z \left[G_d d_2(t) + G_\beta K d_1(t) + G_v v_2(t)\right], \tag{14}$$

where $K = 0.01$ deg/MNm, is a gain that provides appropriate scaling to the signals. The gradient estimate is taken as

$$\begin{aligned}\widehat{\frac{\partial z_1}{\partial \rho}}(\rho^i, t) &= \frac{1}{K}\frac{\partial C_{\text{ff}}}{\partial \rho}(\rho^i) z_2(\rho^i, t) \\ &= \frac{\partial z_1}{\partial \rho}(\rho^i, t) + \frac{1}{K}\frac{\partial C_{\text{ff}}}{\partial \rho}(\rho^i) W_z \left[G_d d_2(t) + G_v v_2(t)\right].\end{aligned} \tag{15}$$

Notice that the disturbances during the gradient experiment corrupt the estimate, but that it is unbiased under the assumption that all noise contributions are zero mean.

2.3.3. Optimization scheme Using the gradient estimate, a gradient-based optimization scheme is implemented to update the controller parameters. Most generally, the parameter update law is expressed as

$$\rho^{i+1} = \rho^i - \gamma^i R(\rho^i)^{-1} \widehat{\frac{\partial J}{\partial \rho}}(\rho^i), \tag{16}$$

where γ^i is the step size, and $R(\rho^i)$ is an approximation of the Hessian. Each of which will now be briefly considered. For the Hessian approximation this work uses

$$R(\rho^i) = H(\rho^i) + \mu \max\left(\text{diag}\left[H(\rho^i)\right]\right) I, \tag{17}$$

where $\mu = 10^{-3}$ is a regularization term to dampen the parameter update, and $H(\rho^i)$ is the Gauss-Newton approximation of the Hessian

$$H(\rho^i) = \frac{2}{N}\sum_{k=0}^{N-1} \widehat{\frac{\partial z_1^i}{\partial \rho}}^{\top}(\rho^i, k) W \widehat{\frac{\partial z_1^i}{\partial \rho}}(\rho^i, k), \tag{18}$$

which is constructed from the signals obtained during second IFT experiment. The step size needs to recede as iterations progress to achieve asymptotic convergence. Therefore

$$\gamma^i = \frac{\eta}{i+\eta}, \tag{19}$$

which is a shifted version of the harmonic series. This work uses $\eta = 5$, which allows the algorithm a larger step size in the earlier iterations.

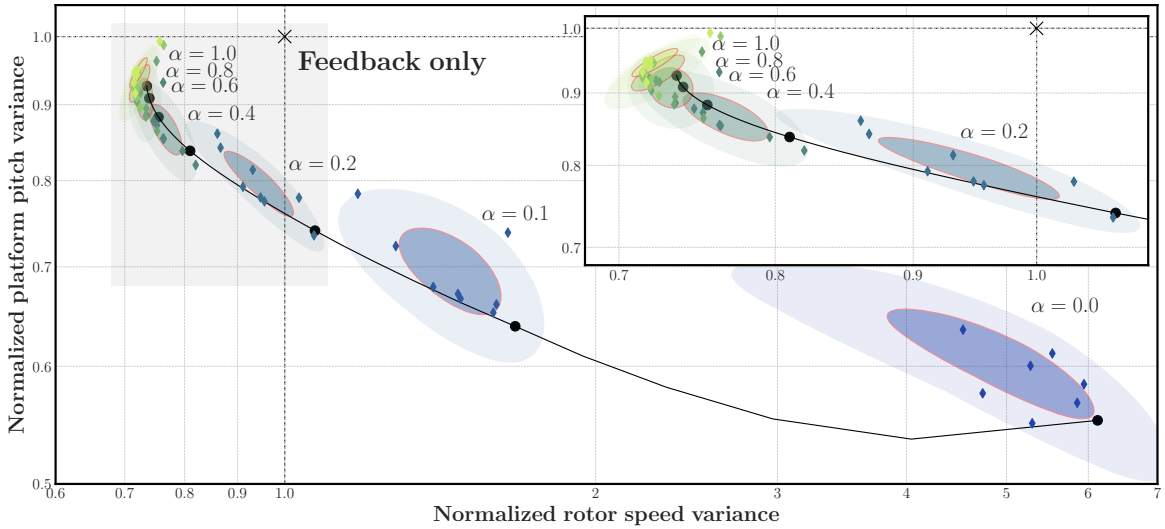


Figure 5: Pareto curve that indicates the possible trade-offs between performing wave feedforward control for the mitigation of rotor speed variance or platform pitch motion. The performance of the optimal controllers obtained with (9) are indicated with the black line, and the performance of the IFT calibrated controllers is indicated with the diamond markers and the ellipsoids. The center of the ellipsoids corresponds the mean of the eight cases considered, and the region that corresponds to 1 and 2 standard deviations is indicated by the ellipsoids.

3. Results

To obtain the results, the IFT algorithm calibrates the controller for 50 iterations, after which a validation experiment with a duration of one hour is performed to assess the performance of the controller. Similarly, the controller obtained from (9) is validated with the same experiment. All experiments are performed with a wind speed of 16 meters per second, and a turbulence intensity of 10%. The wave field is generated according to the JONSWAP spectrum, with a significant wave height of 8.1 meters and a peak period of 12.7 seconds.

To analyze the trade-off between mitigating the wave disturbance from the rotor speed, or the platform pitch angle, the IFT algorithm is deployed for $\alpha \in [0.0, 0.1, 0.2, 0.4, 0.6, 0.8, 1.0]$. To evaluate the convergence of the algorithm, the algorithm is deployed eight times for each value of α. For each of these simulations, a different wind field and wave field is randomly generated, and the algorithm is randomly initialized by drawing parameters from a uniform distribution. The results are presented in Fig. 5 and 6.

In Fig 5, The Pareto front between wave feedforward control for platform pitch and rotor speed is illustrated. In the Pareto front, the normalized variances of the signals obtained from the validation experiments are plotted. The black line indicates the performance of the optimal controllers obtained in Section 2.2.3, and the performance of the IFT controllers are indicated with the ellipsoids. The ellipsoids indicate the mean and the variances corresponding to 1 and 2 standard deviations, which are computed from the multiple IFT runs. Comparing the IFT calibrated controllers to the optimal controllers shows that the IFT algorithm is capable of attaining the performance of the optimal controller for the cases with a small rotor speed variance. From the case $\alpha = 0.2$ it is visible that it is possible to make a trade-off between the performance channels, as for this case the platform pitch variance is reduced with approximately 20% without negatively affecting the variance of the rotor speed. Furthermore, it is visible that in all cases the platform pitch variance improves compared to performing feedback control only.

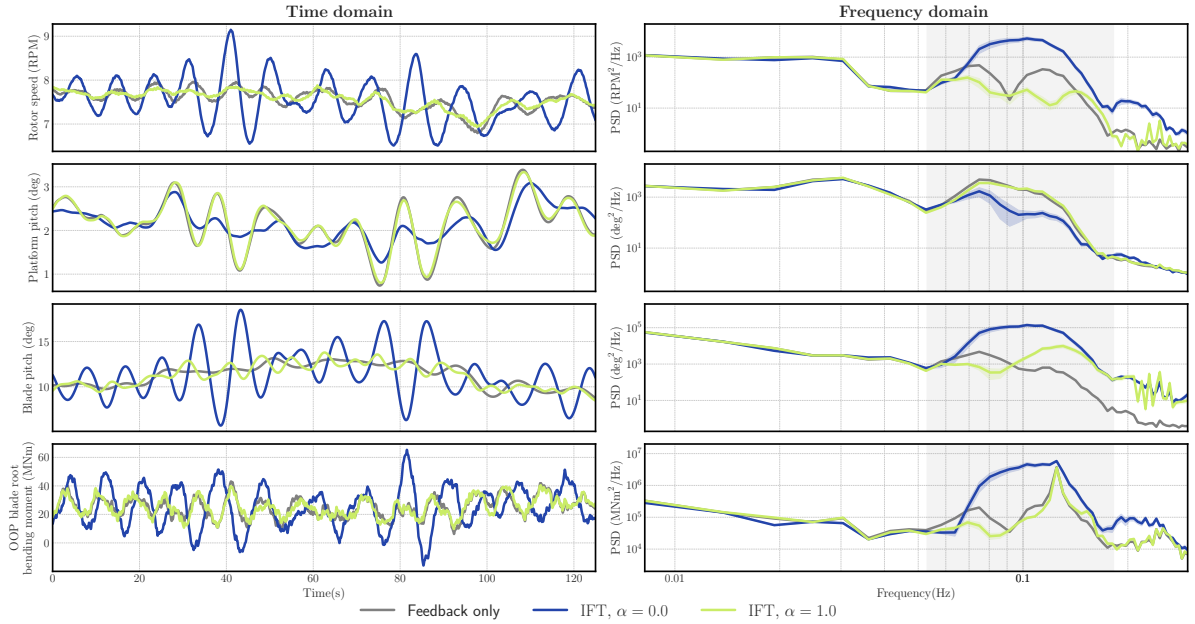


Figure 6: Time domain and frequency domain comparison of the IFT calibrated controllers for $\alpha = 0$ and $\alpha = 1$, to the ROSCO controller. The frequency region where the wave disturbance contains power is highlighted. In the frequency domain plots, the mean of the PSDs is plotted, and the shaded area illustrates the spreading in performance between the eight IFT controllers, and corresponds to one standard deviation.

In Fig. 6, the time and frequency domain responses of the IFT calibrated controllers corresponding to $\alpha = 0$ and $\alpha = 1$, are compared to the case where only feedback control is performed. Next to the rotor speed and platform pitch motion, also the collective pitch angle and the out of plane (OoP) blade root bending moment are considered. From the figure it is clear that the IFT calibrated controllers are effective at mitigating the wave disturbance from the performance channel they were designed for. The figure indicates that performing wave feedforward control to reduce rotor speed variation shows a modest increase in actuation effort, and a decreased OoP blade root bending moment. Performing wave feedforward control to reduce platform pitching motion is effective, but requires high pitch actuation effort, and the pitch controller occasionally exceeds the pitch rate limit of 2 deg/s. Furthermore, this controller shows a significant reduction in the rotor speed tracking, and increased OoP blade root bending moments.

4. Conclusion

This work presented an approach to obtain wave feedforward controllers that combines model-based insights, with data-driven controller calibration with the IFT algorithm. Thereby allowing to obtain optimally calibrated data-driven wave feedforward controllers of user defined complexity. It is concluded that the IFT algorithm accurately calibrates the wave feedforward controllers to a performance criterion that balances rotor speed tracking, and platform pitch motion. Furthermore, it is clear that a trade-off between rejecting the wave disturbance from rotor speed, and the platform pitch motion is possible: the variance of either the rotor speed or the platform pitch motion can be decreased with 25% without negatively affecting the variance of the other performance channel. The feedforward controller calibrated to reject the wave disturbance from the platform motion requires significant pitch actuation, and has detrimental

effects on the OoP blade root bending moment and the rotor speed response. Therefore, it is concluded that the wave feedforward controller is best suited to reject the wave disturbance from the rotor speed, or to control a balanced trade-off between rotor speed tracking and platform pitching motion.

Acknowledgments
This work has received support from the FLOATFARM project, funded by the European Union's Horizon research and innovation program (grant no. 101136091).

References

[1] The European Commission 2020 *An EU Strategy to harness the potential of offshore renewable energy for a climate neutral future* COM/2020/741 final

[2] Messmer T, Ran X, Benifla V, Lutz M, Adam F, Bachynski-Polić E E and Hölling M 2023 Overview of the potential of floating wind in europe based on met-ocean data derived from the era5-dataset *Journal of Physics: Conference Series*

[3] Stockhouse D, Phadnis M, Henry A, Abbas N, Sinner M, Pusch M and Pao L 2023 Sink or swim: A tutorial on the control of floating wind turbines: Preprint (National Renewable Energy Laboratory (NREL), Golden, CO (United States))

[4] Naaijen P and Wijaya A 2014 Phase resolved wave prediction from synthetic radar images (American Society of Mechanical Engineers (ASME)) pp 1–9 ISBN 978-0-7918-4550-9

[5] Ministeru A, Hegazy A and van Wingerden J W 2025 Data-driven wave feedforward control of floating offshore wind turbines *2025 American Control Conference (ACC)* pp 1500–1507

[6] Hegazy A, Naaijen P and van Wingerden J W 2023 Wave feedforward control for large floating wind turbines *Conference on Control Technology and Applications (CCTA)*

[7] Raach S, Schlipf D, Sandner F, Matha D and Cheng P W 2014 Nonlinear model predictive control of floating wind turbines with individual pitch control *2014 American Control Conference* pp 4434–4439

[8] Fontanella A, Al M, van Wingerden J W and Belloli M 2021 Model-based design of a wave-feedforward control strategy in floating wind turbines *Wind Energy Science* **6** 885–901 URL `https://wes.copernicus.org/articles/6/885/2021/`

[9] Hjalmarsson H, Gevers M, Gunnarsson S and Lequin O 1998 Iterative feedback tuning: theory and applications *IEEE Control Systems Magazine*

[10] David M 2020 *QBlade: a modern tool for the aeroelastic simulation of wind turbines* Ph.D. thesis Technische Universität Berlin

[11] Abbas N J, Zalkind D S, Pao L and Wright A 2022 A reference open-source controller for fixed and floating offshore wind turbines *Wind Energy Science*

[12] Hegazy A, Naaijen P, Leroy V, Bonnefoy F, Mojallizadeh M R, Pérignon Y and van Wingerden J W 2024 The potential of wave feedforward control for floating wind turbines: a wave tank experiment *Wind Energy Science*